24th COBEM - 2017

24th ABCM International Congress of Mechanical Engineering
December 3-8, 2017, Curitiba, PR, Brazil

COBEM-2017-1480
Solar Updraft Tower Performance Evaluation

Agustn Ghazarian
Pedro Curto-Risso
Pedro Galione
Instituto Ingenieria Mecanica y Produccion Industrial, Facultad de Ingenieria UDELAR, Julio Herrera y Reissig 565
aghazarian@fing.edu.uy, pgalione@fing.edu.uy,pcurto@fing.edu.uy

Abstract. *The aim of this work is to evaluate the performance of a solar chimney tower in a typical year placed in Uruguay. Solar Updraft Tower consists of a transparent horizontal surface placed at a certain distance above the ground (collector), a tall chimney located in the center of the collector and a turbine at the lower part of the tower. Stack effect, produced by the combination of a temperature difference between inner and outer air and the presence of the chimney, is used for generating air flow through the turbine and producing electric power. This work studies the thermodynamic behavior of the system by a simplified numerical model. Verification and validation of the model is successfully performed, and results of a case study placed in Uruguay are presented.*

Keywords: *Solar Chimneys, Numerical Simulations, Performance Evaluation*

1. INTRODUCTION

World energy consumption is increasing dramatically. The U.S. Energy Information Department predicts that by 2040 the demand will be of 820 quadrillion BTU, that represents a 56% increase from 2010 (524 quadrillion BTU)EIA (2013). Although renewable energy is gaining importance over the years, fossil fuels continue to be the most used energy sourceEIA (2013). However, in order to reverse this reality many new ambient - friendly ways of obtaining energy are being studied all around the world. Particularly, Uruguay is making an important effort to improve its energy matrix. Considering this auspicious environment, the study of new technologies for taking advantage of renewable energy sources seems to be appropriate. The working principle of a Solar Updraft Tower (SUT) consists in using the stack effect in a tall chimney for inducing the motion of air through a turbine, in order to generate electrical power (Fig. 1 extracted from Gannon (2002)). The air is heated using the solar energy trapped inside a collector, consisting on the combination of the ground and a transparent cover, and due to its lower density it escapes through a tall chimney situated in the center of the collector. A turbine connected to a generator, placed at the center of the collector (below the chimney), produces the electrical power. This work studies the performance of a Solar Updraft Tower located in Uruguay, by means of numerical simulation (implemented in C++). One year simulation is ran in order to get different temperatures profiles as well as the plant output power and mass flow.

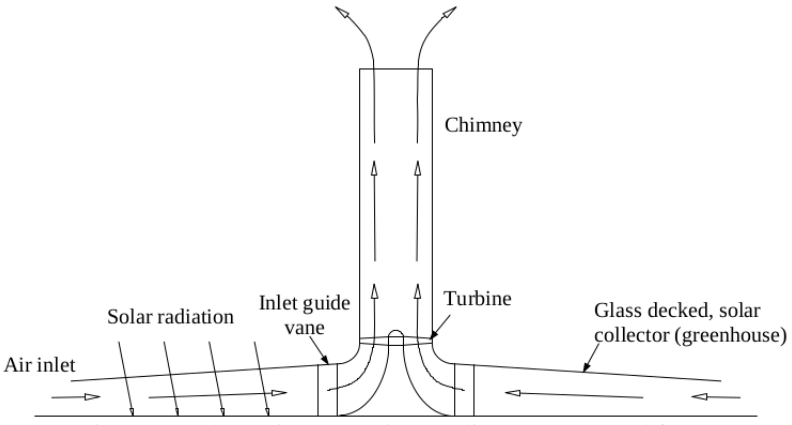

Figure 1: Schematic solar chimney diagram extracted from [2]

2. MATHEMATICAL PROCEDURE

The model consists in solving mass, momentum and energy equations for the circulating air, ground and roof considering the radiation roof-ground exchange. The implemented model is based on the one developed in Pretorius (2004), with some modifications in the correlations used and solving method. Finite volume method was used for the discretization of the equations. The following hypotheses were considered

- One-dimensional flow across the collector and chimney.
- Air flow: one-dimensional, quasi -steady-state. Heat conduction in the flow direction neglected.
- Transient, one dimensional model of ground.
- Imposed ground temperature at certain depth.
- Adiabatic air behavior through the chimney.

At each time step an iterative method is used for solving the coupling of energy and momentum equations and the operating point of the plant can be chosen to follow a maximum power output criteria. In our procedure the collector and chimney pressure drop is solved by integrating the momentum equations along the radius and chimney height.

2.1 Collector model

After applying the simplifying hypothesis the following continuity, momentum and energy expressions for the air mass flow are reached.

$$\frac{1}{r}\frac{\partial}{\partial r}(\rho v r H) = 0 \tag{1}$$

$$H\frac{\partial P}{\partial r} - \tau_r - \tau_g - \frac{F}{r\Delta\theta} = -\rho H v \frac{\partial v}{\partial r} \tag{2}$$

$$h_{rf}A_{roof}(T_{roof} - T_{flow}) + h_{gf}A_{ground}(T_{ground} - T_{flow}) = -\rho H v \frac{\partial (c_p T)}{\partial r} \tag{3}$$

Where r is the control volume radius, v and H the air velocity and collector height at the considered control volume. In eq (2) P represents the pressure, τ_r and τ_g are the roof and ground shear stresses respectively, $F/(r\Delta\theta)$ is a resistive term associated to the geometry structure used to hold the collector and ρ the density. h_{rf} and h_{gf} represent the heat transfer coefficient from the roof and ground to the air flow, A_{ground} and A_{roof} the respective heat exchange areas and T the different temperatures in the control volume presented in figure 2.

As mentioned before, eq.(2) was integrated through all the collector in order to obtain the total pressure drop. For doing this a $H(r)$ function needs to be defined. In order to compare the results reached with the ones obtained in [2,5], the same function was employed, i.e. $H = H_{min}(\frac{r_{max}}{r})^{0.5}$. Dividing eq.(2) by H, re-writing the velocity as function of the mass flow and operating, the following expression is reached:

$$P_{col,in} - P_{col,out} = \dot{m}^2 \int_{r_{min}}^{r_{max}} \frac{1}{A}\frac{\partial}{\partial r}(\frac{1}{\rho A})\delta r - \int_{r_{min}}^{r_{max}} \frac{\tau_r}{H(r)}\delta r - \int_{r_{min}}^{r_{max}} \frac{\tau_g}{H(r)}\delta r - \int_{r_{min}}^{r_{max}} \frac{F}{r\Delta\theta H(r)} \tag{4}$$

Where $A = 2\pi r H(r)$. An extended explanation of τ_r, τ_g and F is presented in [5]. In order to take into consideration the variation with temperature of the thermophysical properties of the air (e.g. ρ and μ), as well as the variation of velocity with r (according to eq. (1)), eq. (4) is numerically integrated between r_{min} and r_{max} through N_{air} control volumes.

Space derivative in Eq. (3), is discretized using a first order upwind scheme in a uniform discretization in the radial direction.

Energy balances to the roof and ground are presented below.

$$\alpha I_h + h_{gr}(T_{ground} - T_{roof}) = h_{ra}(T_{roof} - T_{amb}) + h_{rs}(T_{roof} - T_{sky}) + h_{rf}(T_{roof} - T_{flow}) \tag{5}$$

$$(z_e\alpha_g)I_h = h_{gr}(T_{ground} - T_{roof}) - K_g\frac{\partial T_g}{\partial z} + h_{gf}(T_{ground} - T_{flow}) \tag{6}$$

$$\rho C_p \frac{\delta T}{\delta t} = K_g(\frac{\delta^2 T}{\delta z^2}) \tag{7}$$

Where α is the glass absorptivity (which is calculated depending on the day of the year, time of the day, placement of the chimney and some of the roof properties such as thickness and extinction coefficient) on the other hand h_{gr}, h_{ra} ,h_{rs}, h_{rf}

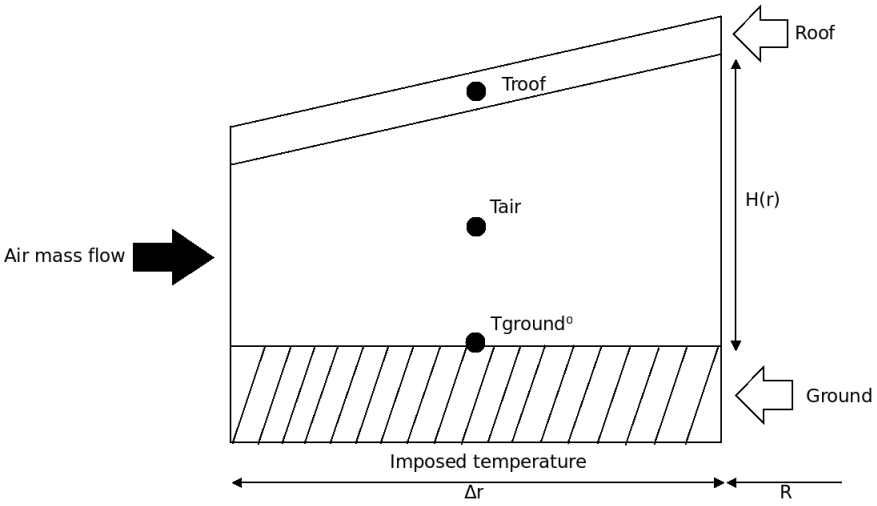

Figure 2: Collector control volumes

and h_{gf} represent the heat transfer coefficient from ground to roof, roof to external air, roof to sky, roof to working fluid and ground to working fluid. $(z_e \alpha_g)$ is the transmittance-absorptivity product which is slightly higher than the product itself due to the many rebounds that makes the energy absorbed higher and finally $K_g \frac{\partial T_g}{\partial z}$ represents the heat lost as conduction into deeper ground. It must be kept in mind that the boundary condition for the the ground solving involves that at certain depth temperature is a fixed parameter.

Space derivative in Eq. (7) is discretized using a second-order centered scheme in a uniform discretization.

2.1.1 Chimney model

In Figure 3 the discretization scheme for the chimney is represented. As expressed earlier inside the chimney no heat transfer is considered, leading to the following continuity, momentum and energy equations.

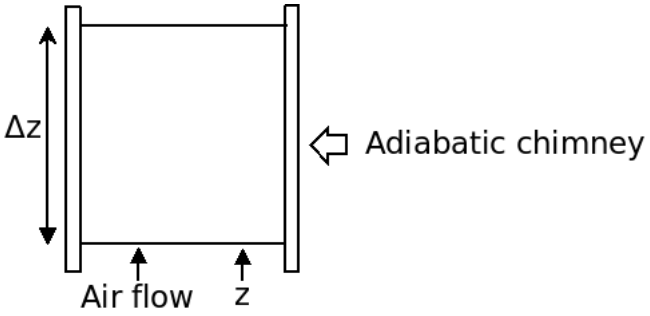

Figure 3: Chimney control volume

$$\frac{\partial(\rho_t v_t)}{\partial z} = 0 \tag{8}$$

$$-\frac{\partial P_t}{\partial z} - \frac{z_t \pi d_t + F_{bw}}{A_t} = \rho_t (g + v_t \frac{\partial v_t}{\partial z}) \tag{9}$$

$$\rho_t \left[v_t \frac{\partial (c_{pt} T_t)}{\partial z} \right] + \frac{\partial(\rho_t v_t g z)}{\partial z} = 0 \tag{10}$$

Where z_t represents the tower shear stress and F_{bw} a resistive force due to bracing wires supporting the tower. For the pressure difference generated in the chimney a similar approach to the one employed in the collector is implemented with the extra facility that the chimney transversal area remains constant, this leads to eq (11).

$$P_{chim,in} - P_{chim,out} = -\int_{z_{min}}^{z_{max}} \rho g dz - \frac{\dot{m}^2}{A_{chim}^2} \int_{z_{min}}^{z_{max}} \frac{1}{\rho} \frac{\partial}{\partial z} \left(\frac{1}{\rho} \right) dz - \frac{1}{A_{chim}} \int_{z_{min}}^{z_{max}} z \pi d_t dz + Fbw \tag{11}$$

Again the whole interval is sub-divided in N_{chim} control volumes, in each of which thermophysical properties may be considered constant.

Here also, the space derivative in the energy equation, Eq. (10), is discretized using a first-order upwind scheme.

2.2 Turbine model

Until now we have presented a simplified model for the working fluid inside the collector and chimney but it is necessary to add the turbine in the analysis as a link between these two parts. There are two terms that must be considered, the temperature drop across the turbine and the pressure drop.

Using that the maximum output power may be calculated as function of the turbine pressure drop and also of the air temperature decay, after some operations eq (12) is obtained

$$T_{t,out} = \frac{(C_p(p_{t,i} + p_{t,o}) - \Delta_{p,turb}R)}{(C_p(p_{t,i} + p_{t,o}) + \Delta_{p,turb}R)} T_{t,in} \tag{12}$$

After assuming a mass flow, the $p_{t,i}$ can be calculated and the rest of the expression can be rewritten in order to depend only of the pressure drop across the turbine that may be solved using an iterative method. The turbine pressure lost is calculated by difference as shown below.

$$\Delta p_{turb} = \Delta p - (\Delta p_i + \Delta p_{coll} + \Delta p_{turb,i} + \Delta p_t + \Delta p_{to} + \Delta p_{dyn}) \tag{13}$$

Where Δp is the driving force generated by the different densities of air in a column of air inside and outside the chimney. By assuming dry adiabatic lapse rate (which involves $T(z) = T_0 - \Gamma z$ with $\Gamma = 0.00975$) for a column of air outside and inside the chimney this driving force can be expressed as follows being H_t the tower height, T_{amb} the ambient temperature and $T_{c,e}$ the temperature at the chimney entrance as shown in Pretorius (2004)

$$\Delta p = p_{amb} \left[1 - \left[\frac{\left(1 - 0.00975 \frac{H_t}{T_{amb}}\right)}{1 - 0.00975 \frac{H_t}{T_{c,e}}} \right]^{3.5} \right] \tag{14}$$

The other terms represent the inlet collector, collector, turbine inlet, tower, tower outlet and dynamic outlet pressure losses.

2.3 Solving Scheme

Collector, chimney and turbine models are combined in order to solve the whole system, following the algorithm shown in Fig (4).

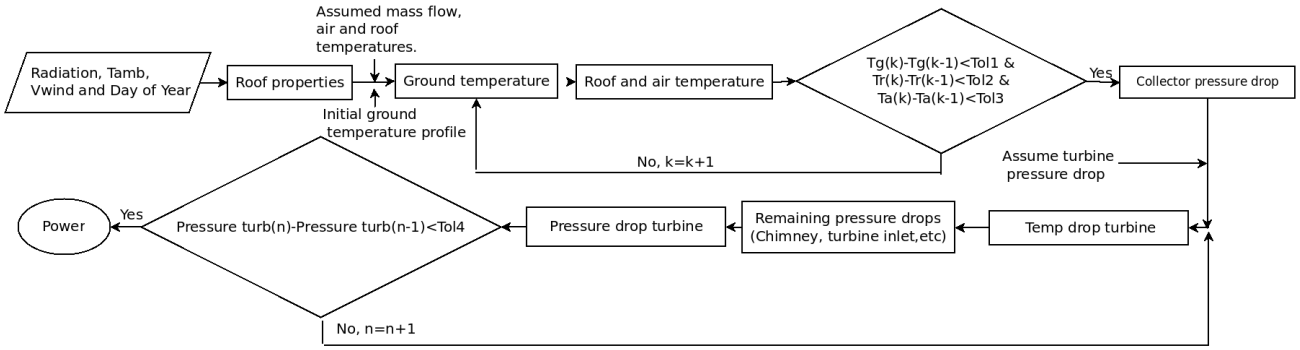

Figure 4: Solver diagram

Firstly, radiation, ambient temperature, wind velocity, specific time of the year and placement of the chimney is introduced. With this information, adding the glass extinction coefficient, thickness and other parameters, the properties of the roof are calculated. For the first time step of iteration, an assumed mass flow and roof profile temperature is introduced along with the initial ground air temperature profile.

As ground temperature is considered to be only a function of depth, a direct tridiagonal method was selected for solving its distribution, due to its simplicity and velocity.

After the ground temperature is known, both air and roof temperature profiles are solved. The resulting system of equations can be represented as a sparse matrix, as shown in Fig (5), which is solved employing a Gauss-Seidel method. With the calculated roof and air temperature, ground temperature is recalculated and this process continues until all of the 3 errors (ground, air and roof) result lower than a certain tolerance.

At this step of the process, the collector temperature profile is solved. After assuming a turbine pressure drop, the air chimney inlet temperature is found. Afterwards, the remaining pressure drops (chimney, outlet, etc.) can be calculated,

which are used to calculate a turbine pressure drop which is compared against the assumed one. These steps are repeated until the difference between the calculated and assumed turbine pressure drops is within a certain tolerance.

Finally, the output power is calculated from the mass flow, turbine pressure drop and turbine efficiency.

The whole-system procedure is repeated for various mass flows in order to find the maximum output power at each time step, assuming that the turbine is operated in order to reach maximum power output. The obtained values are stored to be used in the following time step and the process starts again.

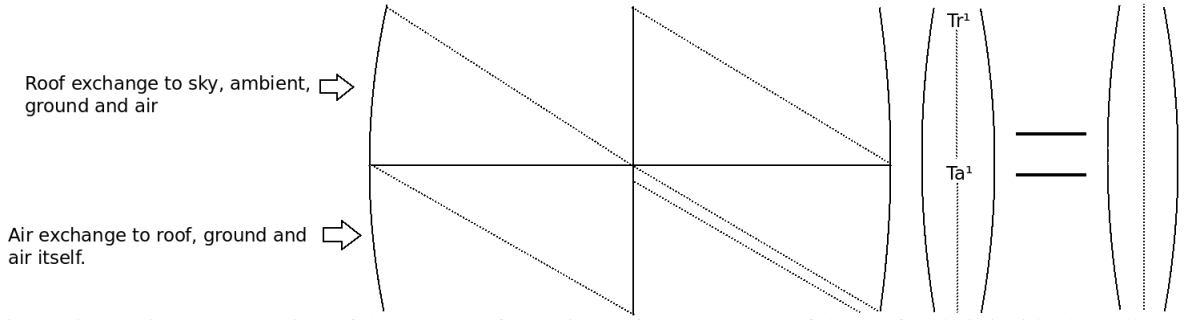

Figure 5: Matrix representation of the system of equations of temperatures of the roof and air inside the collector.

3. Validation

3.1 Simulated plant

As shown in Mullet (1987) for a solar chimney to be efficient large scale models are needed. In order to validate the model the same plant considered in [Gannon (2002) ,Pretorius (2004)] is implemented, the main characteristics are presented below for more information the mentioned papers may be consulted.

- Tower height: 1500 m
- Tower diameter: 160 m
- Collector minimum height: 10 m
- Collector maximum height: 31.6 m
- Collector Radius: 2000 m
- Inside Radius:200 m
- Turbine efficiency: 80%

3.2 Ground and air validation.

In order to verify and validate the model, various steps were followed. The first step consisted in verifying the results of different parts of the code against analytical solutions. The second step consisted in checking the heat gained in the collector (calculated as $Pow = \dot{m}C_p\Delta T$) and ground temperature profiles using experimental data of radiation and ambient temperature (obtained from Haaf (1984)) and comparing it to the experimental measures. Since no wind velocity was informed in Haaf (1984) , a velocity of $0\frac{m}{s}$ was employed. Firstly, a constant ground conductivity was considered, but then an improvement was employed according to conductivity information presented in Haaf (1984) . Variable conductivity has been considered in results shown in figures 6 and 7.

Higher temperatures of the air and ground are obtained in the simulations, which can be caused by the assumption of zero wind velocity, which result in lower thermal losses to the ambient. However, results obtained in this work seem to approximate better the experimental data than those obtained in Gannon (2002) observed in fig (6).

Great agreement between experimental and simulated results is observed , however a higher ground surface temperature and power gained in the collector by the air is noticed at midday. The main explanation is found in the luck of wind velocity information and uncertainty of ground surface conductivity in the data presented.

3.3 Pressure drop verification

For this section a similar approach was implemented. The air mass flow was imposed and every pressure drop was calculated leading to a final turbine pressure drop.The air mas flow was taken from Pretorius (2004) and the resulting

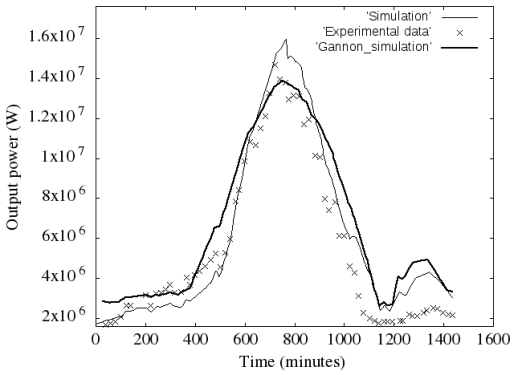

Figure 6: Power gained in the collector

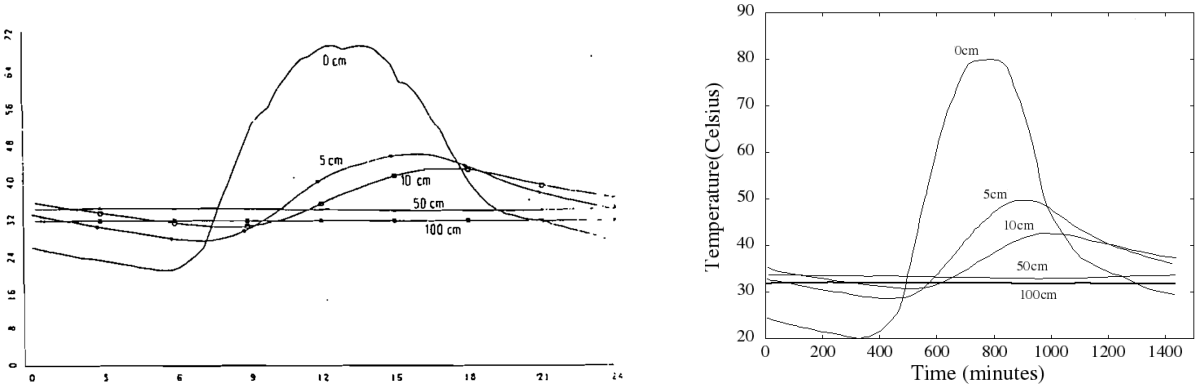

(a) Experimental results extracted from [3]. (b) Numerical results.

Figure 7: Temperature profiles for underground

turbine pressure drop is presented below compared to the one obtained in the mentioned work using similar procedures, losses and heat coefficients. In the mentioned paper not only irradiation and ambient temperature data was provided but also wind velocity information was specified.

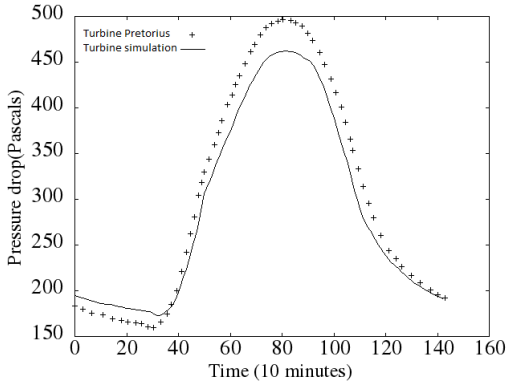

Figure 8: Turbine pressure drop

A 30 Pascals difference can be appreciated at the maximum power production what can be attributed to several factors. To begin with initial conditions may not be the same since in Pretorius (2004) 15 years of operation were simulated in order to reach stationary ground conditions while in our simulation the profile obtained tried to be implemented but with some uncertainties since the temperature profile presented was not too specific. Secondly, different heat and losses coefficients were used and finally the different solving procedure can cause same differences. Anyhow it can be noted that the turbine pressure drop simulated with the in-house code prediction is lower what make us stand on a conservative point.

3.4 Total simulation

The last validation involves considering the maximizing algorithm, this means only ambient conditions will be introduced letting air mass flow as a variable parameter in order to obtain the maximum power at each time step. The result is presented below (in fig 9) overlapped with the power obtained considering the previous mass flow.

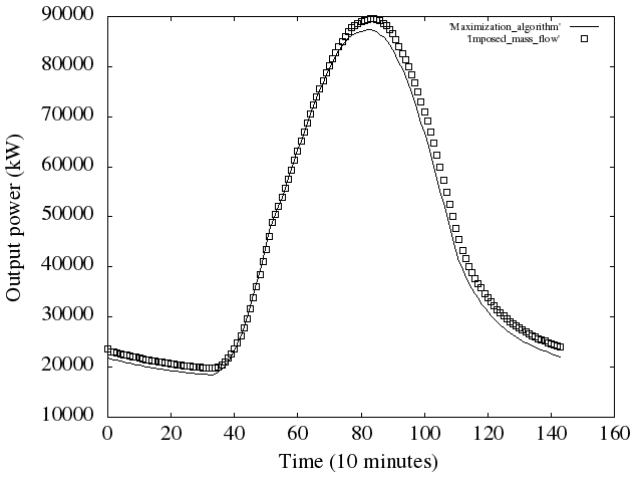

Figure 9: Output power maximization algorithm

Although great agreement can be observed between both simulations, the imposed mass flow is slightly higher what can be explained by the fact that the day shown is the 21st day of simulation but in previous days out algorithm leads to higher output power demanding higher mass flows what cools the ground leading to less energy stored. This situation present a new opportunity of maximization by not extracting the maximum power output every day but maintaining a higher ground temperature that could be released in a posterior day. This approach would not be studied in the current paper.

4. Results

Once the code is validated a simulation using meteorological data from Montevideo extracted from LES (Laboratorio de Energía Solar) was run. Enough years were simulated in order to reach steady-state conditions on the ground profiles over a year. An annual power output results is presented below. As can be seen in the fig(10), peaks of 80MW can be

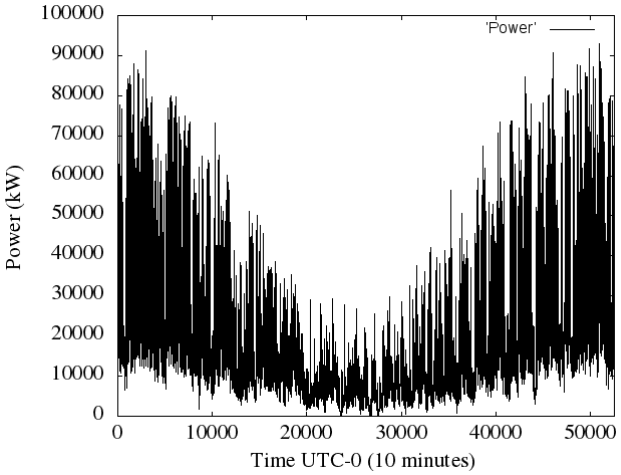

Figure 10: Anual output power

obtained at good irradiative conditions in summer, while at not so good irradiative conditions there are some peaks of about 15MW. Another interesting point is that due to the energy stored in the ground the plant produces energy during the night. At summer this amount is considerable (of about 10 MW).

For a more exhaustive analysis typical output power, temperature profiles and mass flow for a summer and a winter day is shown.

In Fig(11) the power production evolution can be better appreciated. At summer a decay from 20 to 10 MW can be

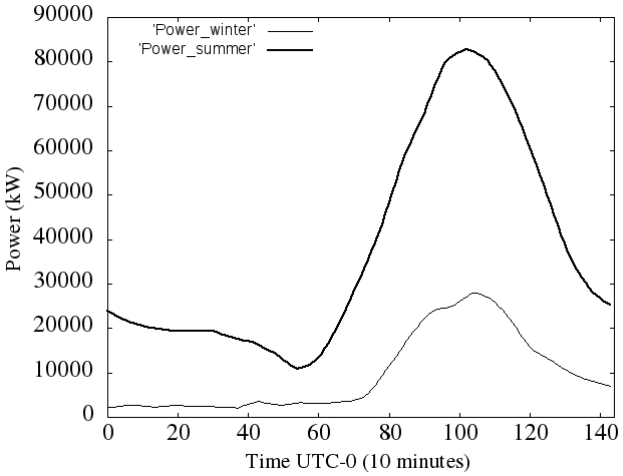

Figure 11: Output power

appreciated during the night due to the ground surface temperature decay, then a 80 MW peak is reached. During winter a constant 3MW production is observed at night and a 20 MW power output is reached.

In fig(12) ground temperature evolution is shown for various depths. In both cases it is observed that the lower layers temperatures (50 and 100 cm) remain almost constant. While in summer at good radiation conditions the higher layers reach higher values reaching a maximum of 335 kelvin in winter the lower layers overcome the top layers. This is explained by the combination of two factors, the ground radiation losses to the roof and the low solar radiation reaching the ground due to not only less incident radiation but also a decrease in the glass transmisivity.

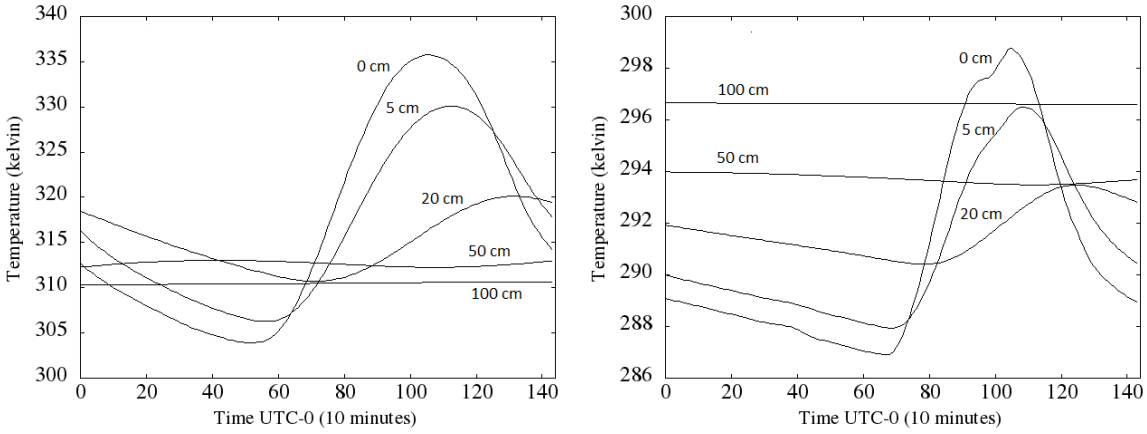

(a) Winter (b) Summer

Figure 12: Temperature profiles of the underground.

As expected, the mass flow evolution goes along with the output power curves reaching top values of 280.000 $\frac{kg}{s}$ and 180.000$\frac{kg}{s}$ in summer and winter respectively as observed in figure (13).

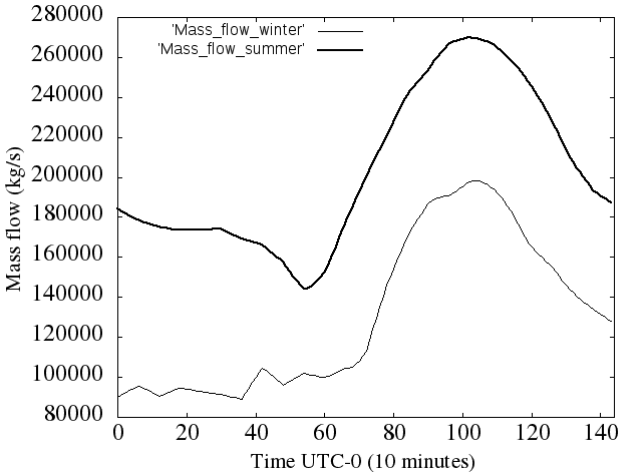

Figure 13: Mass flow

To conclude the analysis an important value to obtain is the overall efficiency. In Mullet (1987) it is shown this concept is proportional to the tower height and concludes that for a tower of 1000m a 1% efficiency is predicted. Calculating the overall efficiency for our large-scale model as follows in eq(14) the following results are reached.

$$\eta = \frac{Power}{A_{col}G} \tag{15}$$

The annual efficiency reaches a value of 0.83% while in summer a winter these values are of 0.89% and 0.68% respectively. These values are among the expected values but to understand better the chimney behavior an instant efficiency calculated as follows is introduced.

$$\eta_{inst} = \frac{Power}{\dot{m}C_p\Delta T_{coll}} \tag{16}$$

This represent the fraction of total energy gained by the air that actually ends up generating electric power. The difference between both efficiencies are the different energy losses present in the plant(radiation to sky,convection to surrounding air, energy lost through the last ground layer and the amount of solar irradiation reflected). Another difference lies in the fact that this efficiency is always lower than unity while at night the first efficiency implemented can not be defined in an instant form. Fig (14) shows this efficiency evolution during a typical year.

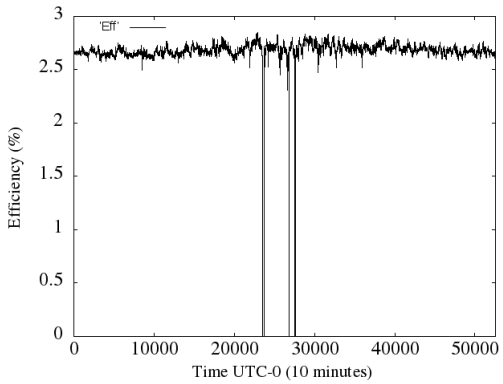

Figure 14: Instant efficiency

This efficiency shows to be fairly constant at a 2.7% value with encourage us to evaluate which one of the mentioned losses is the most significant one. A first way of estimating the total losses is presented below

$$\frac{Pow}{GA_{col}} = \frac{Pow}{\dot{m}C_p\Delta T}\frac{\dot{m}C_p\Delta T}{GA_{col}} \tag{17}$$

$$\frac{Pow}{GA} = 0.83\% \tag{18}$$

$$\frac{Pow}{\dot{m}C_p\Delta T} = 2.7\% \tag{19}$$

and substituting

$$\frac{\dot{m}C_p\Delta T}{GA} = 1 - \frac{losses}{GA} \tag{20}$$

operating a preliminary value of $\frac{losses}{GA} = 0.69\%$ is obtained.
Considering the radiation, convection, reflection loss obtained from the code the obtained value is of 0.691% which is in great agreement with the expected value. After this verification we proceed to obtain the importance of each term in this value. The most significant term is radiation from roof to sky which represents 41.3% of the total input followed by the reflected energy which involves the 19%. The remaining convection term (8.8%) has the particularity of alternating positive and negative values since the roof reaches lower temperatures than the ambient due to it radiative losses. During the analysis the energy lost through the last ground layer was found to be negligible.

5. ACKNOWLEDGEMENTS

This work was supported by the ANII (Agencia Nacional de Investigación e Innovación) through project FSE_2014_1_102106.

6. REFERENCES

EIA, 2013. "Today in energy". <https://www.eia.gov/todayinenergy/detail.php?id=12251.>.
Gannon, A., 2002. *Solar Chimney Turbine Performance*. Ph.D. thesis, University of Stellenbosch, Stellenbosch.
Haaf, W., 1984. "Solar chimneys". *International Journal of Solar Energy*, pp. 141–161.
Mullet, L., 1987. "The solar chimney overall efficiency, design and performance". *International Journal of Ambient Energy*, pp. 35–40.
Pretorius, J., 2004. "Solar tower power plant performance characteristics".

7. RESPONSIBILITY NOTICE

The authors is are the only responsible for the printed material included in this paper.